



Petahertz-scale nonlinear photoconductive sampling in air

DMITRY ZIMIN,^{1,2} MATTHEW WEIDMAN,^{1,2,4} JOHANNES SCHÖTZ,^{1,2} MATTHIAS F. KLING,^{1,2}  ID
VLADISLAV S. YAKOVLEV,^{1,2}  ID FERENC KRAUSZ,^{1,2} AND NICHOLAS KARPOWICZ^{1,3,*}

¹Max-Planck-Institut für Quantenoptik, Hans-Kopfermann-Strasse 1, 85748 Garching, Germany

²Fakultät für Physik, Ludwig-Maximilians-Universität, Am Coulombwall 1, 85748 Garching, Germany

³CNR NANOTEC Institute of Nanotechnology, via Monteroni, 73100 Lecce, Italy

⁴e-mail: matthew.weidman@mpq.mpg.de

*Corresponding author: nicholas.karpowicz@nanotec.cnr.it

Received 30 September 2020; revised 17 February 2021; accepted 26 February 2021 (Doc. ID 411434); published 26 April 2021

The electric field waveform of a light field can be used to unlock a detailed recording of its interaction with matter, but accessing it requires a measurement with subfemtosecond temporal resolution. We demonstrate nonlinear photoconductive sampling of light fields at optical frequencies in ambient air. The resulting detection method provides broadband electric field measurement in an inexpensive setup using a self-healing medium. A direct comparison is made between detection in air and in quartz, validating the technique up to 0.7 PHz. This provides both a simple route toward field metrology and a new platform for future studies in attosecond physics without the need for complex vacuum setups or sophisticated sample preparation. © 2021 Optical Society of America under the terms of the [OSA Open Access Publishing Agreement](#)

<https://doi.org/10.1364/OPTICA.411434>

1. INTRODUCTION

The electric field waveform of light carries with it a detailed description of the internal dynamics of the atoms, molecules, or solids it encountered on its way to the detector. To fully unlock this information, strict prerequisites in measurement bandwidth and sensitivity must be met. An attempt to directly measure a time-varying field, using a state-of-the-art oscilloscope with 70 GHz analog bandwidth, constitutes the bandwidth limit of conventional electronic metrology—on the order of 0.1 THz [1]. The detection of field transients at frequencies beyond this limit was demonstrated by Auston *et al.* in 1980 [2], in which the researchers leveraged picosecond laser pulses to generate a temporal gate, thus marking the beginning of terahertz-frequency optoelectronics. This measurement capability led to the development of time domain spectroscopy at terahertz frequencies [3–6], a spectral range within which materials present rotational and vibration signatures. To measure fields that oscillate near petahertz frequencies, within the optical spectral region, a faster—ideally subfemtosecond—temporal gate is needed. During the quest for subfemtosecond pulses, there were many advances in laser technology before a paradigm shift ultimately led to the generation of the first isolated attosecond pulses in 2001 [7–10], obtained through high-harmonic generation. The use of attosecond pulses to provide a subfemtosecond temporal gate has for nearly two decades routinely allowed time-varying fields to be measured at optical frequencies [7,11,12]. This measurement bandwidth has, within a vacuum environment, enabled a myriad of new possibilities for triggering and measuring subfemtosecond dynamics

within materials. For example, *attosecond polarization spectroscopy* [13] translates the modifications of the structure of the waveform into a high-resolution recording of light–material interaction at petahertz frequencies. Because materials absorb light over a spectral bandwidth from gigahertz/terahertz (rotational and vibrational resonances) to petahertz (electronic resonances), field sampling that leverages multioctave detection bandwidth while also providing high sensitivity and dynamic range has great potential for future attosecond and femtosecond experiments.

The same advances in laser technology that contributed to the birth of attosecond physics have been crucial for the advancement of other field sampling techniques toward petahertz frequencies that do not rely on attosecond pulses from high-harmonic generation. The extension of electro-optic sampling (EOS) has benefited from the capability of compressing broad spectral bandwidths and has been demonstrated for the detection of pulses at frequencies up to 0.25 PHz in 2016 [14] and field transients at frequencies up to 0.4 PHz in 2017 [15]. Although the sensitivity and dynamic range of EOS are appealing [16], the direct extension of this technique towards multipetahertz frequencies would require a probe pulse with twice the frequency of field to be sampled and its near-dispersion-free propagation through an extended, macroscopic medium—a major challenge.

For field measurements in air, an alternative was demonstrated in 2018 up to 0.6 PHz, the tunneling ionization with a perturbation for the time-domain observation of an electric field (TIPTOE) method [17]. It uses the perturbation of strong-field ionization by a superimposed weak field, both polarized in the same direction, in

order to resolve the electric field of the perturbing pulse, albeit with an ambiguity in the sign of the field unless the carrier-envelope phase of the strong field is known. The resulting charges are collected with a pair of electrodes with applied bias. An alternative approach, nonlinear photoconductive sampling (NPS) exploits the sudden change in electron *mobility* upon highly nonlinear photoionization, thus providing a subfemtosecond temporal gate for measuring the time-dependent electric field of a driving pulse, which accelerates the charges. In contrast to TIPTOE, the dependence of the ionization probability on the delay between the ionizing and driving pulses is insubstantial for NPS. This technique was demonstrated for field detection at frequencies exceeding 1 PHz, first using a quartz sample [18]. In a parallel but independent effort, an implementation of field sampling in air was reported for frequencies of 0.13 PHz [19]. In this work, we show that a near-petahertz detection bandwidth is also achievable with nonlinear photoconductive sampling in air. By benchmarking against NPS in solids, we show that NPS in air constitutes a viable alternative to NPS in solids throughout the visible spectrum.

2. EXPERIMENTAL

The experiments were performed with a femtosecond laser that is reported in detail elsewhere [18]. In brief, a Ti:Sapphire chirped pulse amplifier at a repetition rate of 3 kHz provided 21-fs pulses with 2.5-W average power. The pulses were spectrally broadened in a hollow-core fiber (HCF) and compressed using chirped mirrors to 2.6 fs (full width at half-maximum), characterized in previous experiments via NPS [18]. For field sampling, the pulses were separated into two arms in a Mach-Zehnder interferometer configuration (see Supplement 1). These two pulses, dubbed “injection” and “drive,” were given orthogonal polarizations with a variable time delay with respect to each other [Fig. 1(a)]. The stronger injection pulse, which was vertically polarized, ionized ambient air, creating free electrons. Because the injection pulse was polarized along the direction of the electrodes, it did not by itself generate a signal. The weak drive pulse was polarized across

the electrodes and was responsible for signal generation by displacing electrons toward one of the electrodes. As the drive pulse separates electrons from positively charged ions, the emerging dipole induces image charges in the electrodes, inducing/driving a measurable current in a simple external circuit [Fig. 1(a)]. A transimpedance amplifier was used to provide a voltage in response to an input current. For the case of NPS in solids, this current was found to be proportional to the vector potential of the drive field [18].

In the case of a gap, the induced current can be interpreted as an imbalance in the angle-resolved photoemission of electrons in the half-planes defined by the electrodes. This asymmetry is the result of the combined action of the laser fields and the Coulomb potential of the ion on the electron, which can be simulated through solution of the time-dependent Schrödinger equation (TDSE), as shown in Figs. 1(b) and 1(c) for the example of a hydrogen atom. In the absence of a driving field, the asymmetry is only in the direction of the injection field, which produces a photoemission pattern that is identical in the planes of the two electrodes. In the presence of a driving field, the photoemission is modified such that an asymmetry appears, resulting in a measurable potential between the electrodes, as can be seen in Fig. 1(c).

By scanning the time delay between the nonlinear injection of carriers (the time gate) and the field to be traced/sampled (drive pulse), the electric field could be retrieved [Fig. 2(a)]. Here, this was done for NPS in fused silica [Fig. 2(a), red curve] for comparison to NPS in air [Fig. 2(a), blue curve].

From the retrieved electric field, the spectral amplitude [Fig. 2(b), blue and red] and phase [Fig. 2(b), green and orange] of the pulse were calculated for NPS in air and SiO₂, respectively. The standard deviation of five measurements in both air and fused silica is represented by the shaded areas in Fig. 2(b). A typical measurement time for a complete trace is several minutes. An extensive benchmarking of the spectral behavior was performed for NPS for the case of solids in Ref. [18] in various spectral ranges.

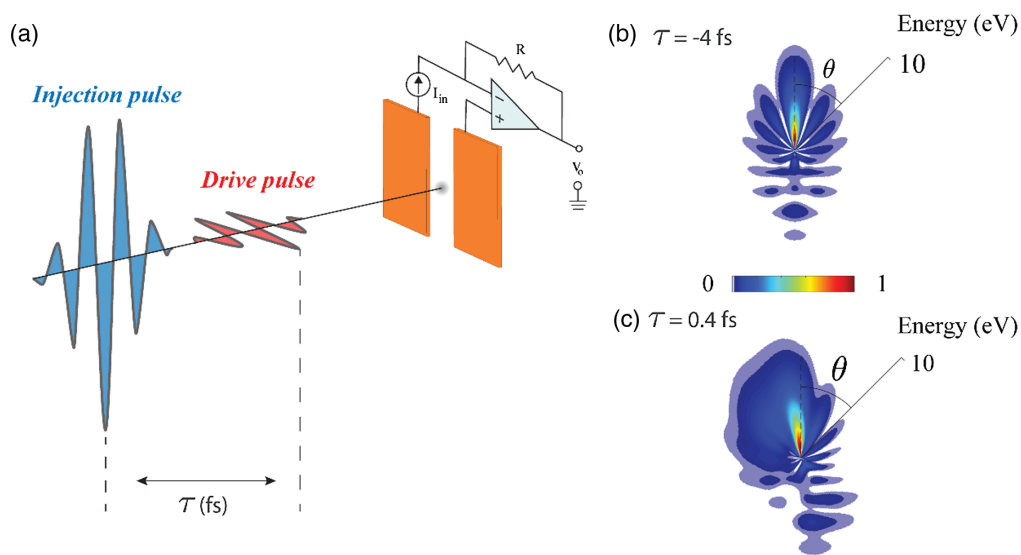


Fig. 1. NPS in air. (a) A vertically polarized *injection* pulse with sufficient intensity to generate free carriers is collinearly superposed with a horizontally polarized weak *drive* pulse. The panels on the right show the (b) unperturbed and (c) perturbed angle-resolved energy distributions of the free electrons released by a vertically polarized, 15-GV/m, 2.2-fs pulse in hydrogen, obtained by solving the TDSE. The horizontally polarized optical field (3 GV/m amplitude) causes an imbalance in the direction of the electrodes (a), which is maximal at $\tau = 0.4$ fs for the pulse pair employed. The electrodes screen the resulting dipole, inducing a current in the measurement circuit.

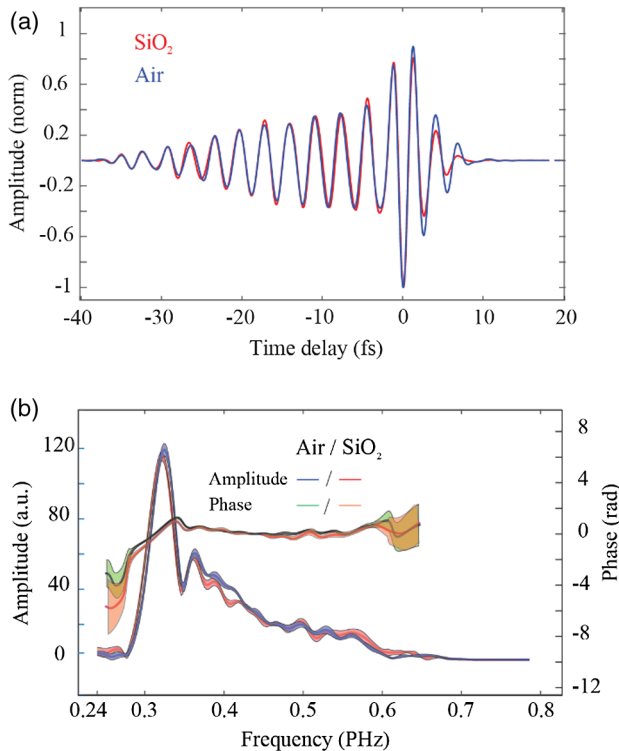


Fig. 2. (a) Comparison of the NPS measurements in air (blue trace) and in SiO_2 (red trace); (b) spectral amplitudes and phases obtained by taking the Fourier transform of the electric fields shown in (a).

3. SIMULATIONS

The mechanism for the generation of a discernible signal from NPS in air at ambient pressure is analogous to the application of NPS in solids: the separation of charges leading to the formation of a dipole [19], whose field is screened by the metal electrodes, ultimately forming a current in the external circuit. Based on the number density of air at atmospheric pressure, and the corresponding mean-free-path of the ionized electrons ($< 1 \mu\text{m}$), it is unlikely that a significant number of photoelectrons can reach the electrodes, which are separated by an $\sim 80 \mu\text{m}$ gap. Nevertheless, the electron mean-free-path in gases is significantly higher than that in solids, leading to a larger displacement of the electrons, which could explain why similar signal strengths (measured field amplitudes within a factor of 2) are observed in both media, despite the strongly differing carrier densities.

For any electric-field measurement, it is vital to understand the relationship between the measured waveform and the true electric field. In photoionization of atoms and molecules, a possible confounding factor is the Coulombic potential surrounding the parent ion, which will cause the free-electron motion to deviate from the predictions of the strong-field approximation (SFA), according to which a signal is proportional to the vector potential of the drive field convolved with the gate function produced by the photoionization event. In order to investigate the influence of the Coulomb field of the parent ion on the measured signal, we numerically solved the TDSE in three spatial dimensions (see Supplement 1), using hydrogen as a model atom. This is justified since, although differences in short-range potential are certainly to be expected for different gas species, the long-range interaction rapidly converges to Coulombic over the majority of the space occupied by the electron wave packet as it interacts with the field.

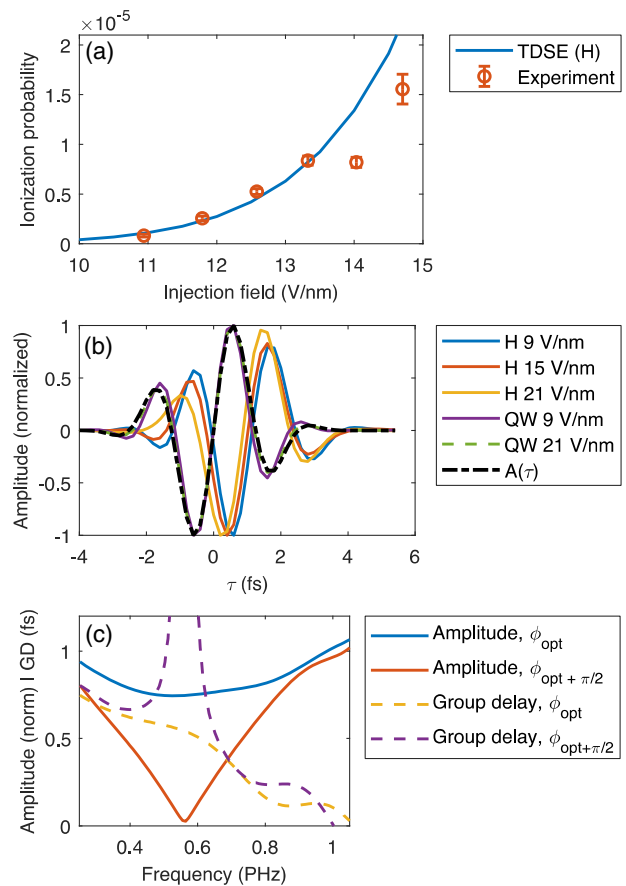


Fig. 3. Intensity scaling and time-domain response of the measurement process, as simulated by solving the TDSE for a hydrogen atom in the range from 10 to 15 GV/cm ($1.3 - 3.0 \times 10^{13} \text{ W/cm}^2$ intensity). (a) Measured intensity scaling of the signal compared with the ionization probability for several peak strengths of the injection field; (b) the measurement process is simulated as the appearance of a delay-dependent asymmetry in the angle-resolved photoelectron momentum distribution. In the presence of the atomic potential, the measurement reproduces the vector potential of the applied electric field, with a delay and phase shift caused by Coulomb–laser coupling. As expected, this delay is intensity-dependent, as higher intensities yield higher energy photoelectrons, which are less sensitive to the potential. Performing the same simulation in an isolated spherical quantum well (QW)—a short-range potential with a single bound state of 13.6 eV binding energy—yields a similar trace, but with vanishing phase shift. Positive values of τ signify that the drive field comes before the injection pulse. (c) Simulated amplitude response and group delay of the measurement for the optimal carrier-envelope phase (CEP) and the optimal CEP plus $\pi/2$, which exhibits a distinct minimum near the carrier frequency of the injection pulse. This provides a numerical correction that can be applied to the measurement results to link them to the true electric field.

Figure 3 shows a comparison of the ionization probability obtained from the TDSE and the measured signal, which shows qualitative agreement until the presence of a denser gas plasma perturbs the intensity scaling.

Our signal is dominated by low-energy electrons, whose dynamics and interaction with the laser is influenced by the presence of the atomic/ionic potential. As in attosecond streaking experiments, where electrons are created through linear photoemission using a weak XUV pulse, the two main effects that influence the relative timing of the streaking signal are the atom-specific Wigner delay and Coulomb–laser-coupling (CLC).

For low-energy electrons (below 10 eV), the magnitude of these effects on the timing is expected to be several 100 as [20–23]. The electrons undergo ponderomotive motion in the relatively strong injection field direction while they are being accelerated by the drive field, leading to a more complicated CLC in our case. Nevertheless, similar delays as in attosecond streaking are to be expected.

Using the TDSE to calculate the measured signal, assumed to be proportional to the momentum asymmetry of the resulting angle-dependent photoelectron spectrum in the direction of the drive field, we see that the signal as a function of time delay approximates the vector potential of the drive field, but with a significant delay. We attribute this delay to CLC, and it agrees in magnitude with analytical theories developed for attosecond streaking [21]. To further verify this, the potential of the hydrogen ion in the simulation was replaced with a short-range spherical quantum well with a single 13.6 eV bound state. The short-range potential results in a signal that is in very good agreement with the SFA and with no appreciable delay. The effect of CLC varies in strength with the intensity of the injection field, due primarily to the injection of higher-energy electrons at higher intensities, which are less sensitive to the field of the parent ion.

The feasibility of first-principle simulations of the microscopic interaction allows for the microscopic response function to be fully characterized. This results in the spectral amplitude and group delay variations, with frequency shown in Fig. 3(c). Appropriate phase and amplitude adjustments should be made to the measured signal if one wishes to accurately characterize the temporal evolution of the drive field in attosecond experiments. At high pressures and higher ionization rates, macroscopic effects may also affect the measurement, in terms of propagation of both the pulses being measured (plasma dispersion and the Kerr effect), and the motion of the free electrons (collisions, collective plasma oscillations, and space charge) in the medium [24].

4. DISCUSSION

Although NPS in solids benefits from a bandgap energy that is less than the ionization potential of most gases, NPS in gases offers several potential advantages over NPS in solids. The fabrication of the sample is simplified, since deposition of electrodes on the solid sample is not required, making the technique even more accessible. Additionally, the injection intensity is not limited by the damage threshold of the solid, and the medium is self-healing. Finally, the well-established theory and existing models for strong-field ionization dynamics in atoms and molecules, such as numerical solution of the TDSE or Coulomb-corrected SFA, make the interpretation of the signal more straightforward.

Experimentally, the optimum conditions, in which the required spectral amplitude and phase corrections are minimal, should be obtained by finding the value of the CEP, which maximizes the measured signal [see Fig. 3(c)]. This corresponds to the condition where the photoemission gate is maximally confined to a single half-cycle of the injection field. Calculation of the Coulomb-induced phase correction is best performed using a measured injection pulse. If CEP optimization is performed experimentally, this can be obtained through standard techniques that yield the complex envelope function, such as frequency-resolved optical gating (FROG). As with other field measurement techniques, the obtained waveform is the convolution of the actual field with a gate function corresponding to the physical response of the system,

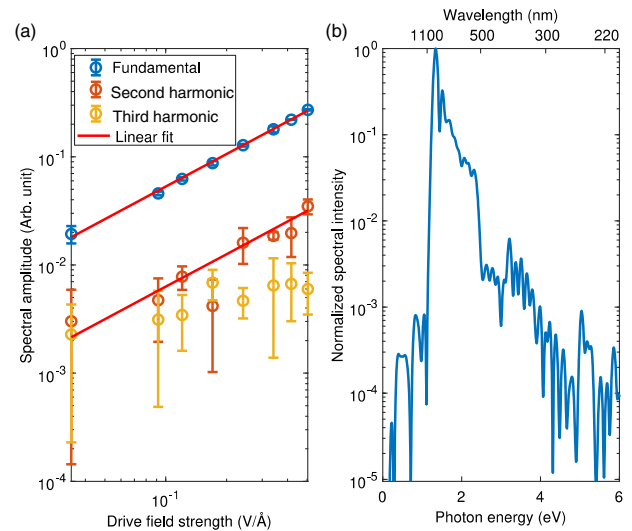


Fig. 4. (a) Linearity of the detection and noise level indicated by the spectral components of the waveform at 300–344 THz (fundamental), 688–733 THz (second harmonic) and 957–1000 THz (third harmonic) obtained by Fourier transformation of the measured signals at varying drive field strengths, with an injection field strength of 1.1 V/Å; (b) logarithmically scaled spectrum and spectral noise floor in the visible spectral range measured with an injection field strength of 1.1 V/Å and drive field of 0.26 V/Å.

whose influence must be corrected if one wishes to obtain the true electric field. In the case of NPS in gases, especially in the case of simpler noble gases, doing this in an *ab initio* manner is feasible.

To examine the signal-to-noise ratio (SNR) and linearity of the signal with the measured field, we show the dependence of the signal at the fundamental frequency of the drive field, as well as two harmonic multiples of that frequency, as a function of drive field strength. This set of data allows for two important aspects of the measurement to be observed simultaneously. In the case in which there is no component of the drive field at the harmonic frequencies, this allows for sensitive detection of harmonic distortions that would result from nonlinearity in the detection. In the range of intensities applicable in the experiment, distortions from, e.g., the drive field significantly altering the ionization probability in the experiment, were absent. Such harmonics would be expected to grow with a nonlinear dependence on field strength. In the case of detection of the fundamental pulse [Fig. 4(b)], the signal at the second harmonic grows linearly, indicative of linear field detection of the weak ~ 400 nm signal reflected outside of the working spectral range of the chirped mirrors. A similar trend was observed when characterizing NPS in solids [18]. The amplitude at the third harmonic does not contain any measurable signal and is indicative of the noise floor of the experiment. The SNR in the range of intensity is above 100 in terms of intensity. This can also be seen intuitively in the logarithmically scaled spectrum [Fig. 4(b)] obtained via Fourier transformation of the experimentally retrieved waveform [Fig. 2(a), blue curve], where the amplitude falls abruptly outside of the working spectral range of the chirped mirror compressor (Ultrafast Innovations PC1491, 500–1050 nm).

5. CONCLUSION AND OUTLOOK

We have presented a simple and versatile technique for sampling light fields at frequencies in the petahertz range: nonlinear

photoconductive sampling in air. While NPS in solids has potential for future implementation within optoelectronic devices and is suitable for lower-energy injection pulses, the implementation of NPS in gas, complementary to attosecond measurements using XUV pulses, permits a physical interpretation based on first principles. Our simulations show that NPS in gases could also provide an interesting route to attosecond field-resolved spectroscopy involving low-energy electrons, e.g., for time-resolving photoionization processes where the Coulomb interaction between an electron and its parent ion plays the dominant role.

Funding. Tecnopolo di Nanotecnologia e Fotonica per la medicina di precisione (TECNOMED)—FISR/MIUR-CNR: (CIPE n.3449 del 7-08-2017, CUP: B83B17000010001); Technomed Puglia (CUP: B84I18000540002, DGR n.2117 del 21/11/2018); King Abdullah University of Science and Technology (OSR-2016-CRG5-2995); Laserlab Europe (EU-H2020 654148); European Research Council (FETopen PetaCOM); Air Force Office of Scientific Research (FA9550-14-1-0389, FA9550-16-1-0073, FA9550-16-1-0156); Deutsche Forschungsgemeinschaft (KL-1439/11-1).

Disclosures. The authors declare no conflicts of interest.

Supplemental document. See Supplement 1 for supporting content.

REFERENCES

- X. Chen, S. Chandrasekhar, S. Randel, G. Raybon, A. Adamecki, P. Pupalaiakis, and P. J. Winzer, "All-electronic 100-GHz bandwidth digital-to-analog converter generating PAM signals up to 190 GBaud," *J. Lightwave Technol.* **35**, 411–417 (2017).
- D. Auston, A. Johnson, P. Smith, and J. Bean, "Picosecond optoelectronic detection, sampling, and correlation measurements in amorphous semiconductors," *Appl. Phys. Lett.* **37**, 371–373 (1980).
- D. Grischkowsky, S. Keiding, M. Van Exter, and C. Fattinger, "Far-infrared time-domain spectroscopy with terahertz beams of dielectrics and semiconductors," *J. Opt. Soc. Am. B* **7**, 2006–2015 (1990).
- S. Nishizawa, K. Sakai, M. Hangyo, T. Nagashima, M. W. Takeda, K. Tominaga, A. Oka, K. Tanaka, and O. Morikawa, "Terahertz time-domain spectroscopy," in *Terahertz Optoelectronics* (Springer, 2005), pp. 203–270.
- P. Han, M. Tani, M. Usami, S. Kono, R. Kersting, and X.-C. Zhang, "A direct comparison between terahertz time-domain spectroscopy and far-infrared Fourier transform spectroscopy," *J. Appl. Phys.* **89**, 2357–2359 (2001).
- J. Neu and C. A. Schmuttenmaer, "Tutorial: an introduction to terahertz time domain spectroscopy (THz-TDS)," *J. Appl. Phys.* **124**, 231101 (2018).
- F. Krausz, *Electrons in Motion* (World Scientific, 2019).
- F. Krausz and M. Ivanov, "Attosecond physics," *Rev. Mod. Phys.* **81**, 163 (2009).
- M. Drescher, M. Hentschel, R. Kienberger, G. Tempea, C. Spielmann, G. A. Reider, P. B. Corkum, and F. Krausz, "X-ray pulses approaching the attosecond frontier," *Science* **291**, 1923–1927 (2001).
- M. Hentschel, R. Kienberger, C. Spielmann, G. A. Reider, N. Milosevic, T. Brabec, P. Corkum, U. Heinzmann, M. Drescher, and F. Krausz, "Attosecond metrology," *Nature* **414**, 509–513 (2001).
- E. Goulielmakis, M. Uiberacker, R. Kienberger, A. Baltuska, V. Yakovlev, A. Scrinzi, T. Westerwalbesloh, U. Kleineberg, U. Heinzmann, M. Drescher, and F. Krausz, "Direct measurement of light waves," *Science* **305**, 1267–1269 (2004).
- K. T. Kim, C. Zhang, A. D. Shiner, B. E. Schmidt, F. Légaré, D. Villeneuve, and P. Corkum, "Petahertz optical oscilloscope," *Nat. Photonics* **7**, 958–962 (2013).
- A. Sommer, E. Bothschafter, S. Sato, C. Jakubeit, T. Latka, O. Razskazovskaya, H. Fattahi, M. Jobst, W. Schweinberger, V. Shirvanyan, V. Yakovlev, R. Kienberger, K. Yabana, N. Karpowicz, M. Schultze, and F. Krausz, "Attosecond nonlinear polarization and light-matter energy transfer in solids," *Nature* **534**, 86 (2016).
- S. Keiber, S. Sederberg, A. Schwarz, M. Trubetskov, V. Pervak, F. Krausz, and N. Karpowicz, "Electro-optic sampling of near-infrared waveforms," *Nat. Photonics* **10**, 159–162 (2016).
- O. Razskazovskaya, "Infrared waveform synthesis for applications in attosecond science," *Faculty of Physics*, Munich, Germany, LMU München, 2017.
- A. Leitenstorfer, S. Hunsche, J. Shah, M. Nuss, and W. Knox, "Detectors and sources for ultrabroadband electro-optic sampling: experiment and theory," *Appl. Phys. Lett.* **74**, 1516–1518 (1999).
- S. B. Park, K. Kim, W. Cho, S. I. Hwang, I. Ivanov, C. H. Nam, and K. T. Kim, "Direct sampling of a light wave in air," *Optica* **5**, 402–408 (2018).
- S. Sederberg, D. Zimin, S. Keiber, F. Siegrist, M. S. Wismer, V. S. Yakovlev, I. Floss, C. Lemell, J. Burgdörfer, M. Schultze, F. Krausz, and N. Karpowicz, "Attosecond optoelectronic field measurement in solids," *Nat. Commun.* **11**, 1–8 (2020).
- A. Korobenko, K. Johnston, M. Kubullek, L. Arissian, Z. Dube, T. Wang, M. Kübel, A. Y. Naumov, D. Villeneuve, M. Kling, P. Corkum, A. Staudte, and B. Bergues, "Femtosecond streaking in ambient air," arXiv:2005.10952 (2020).
- M. Ivanov and O. Smirnova, "How accurate is the attosecond streak camera?" *Phys. Rev. Lett.* **107**, 213605 (2011).
- R. Pazourek, S. Nagele, and J. Burgdörfer, "Attosecond chronoscopy of photoemission," *Rev. Mod. Phys.* **87**, 765 (2015).
- A. S. Landsman and U. Keller, "Attosecond science and the tunnelling time problem," *Phys. Rep.* **547**, 1–24 (2015).
- O. Kullie, "Tunneling time in attosecond experiments and the time-energy uncertainty relation," *Phys. Rev. A* **92**, 052118 (2015).
- J. Schötz, B. Förg, W. Schweinberger, I. Liontos, H. Masood, A. Kamal, C. Jakubeit, N. Kling, T. Paasch-Colberg, S. Biswas, M. Högnér, I. Pupeza, M. Alharbi, A. Azzeer, and M. Kling, "Phase-matching for generation of isolated attosecond XUV and soft-X-ray pulses with few-cycle drivers," *Phys. Rev. X* **10**, 041011 (2020).